Structural complexity of Y_6BO_{12} fluorite-related ternary oxides

Gianguido Baldinozzi[1], Luis Casillas-Trujillo[2], Maulik K. Patel[3], Kurt E. Sickafus[4]

[1] Structures, Propriétés et Modélisation des Solides, Université Paris Saclay, CNRS, Centralesupélec, 91190 Gif-sur-Yvette, France. gianguido.baldinozzi@centralesupelec.fr
[2] IFM, Linköping University, SE-581 83 Linköping, Sweden.
[3] Department of Mechanical, Materials and Aerospace Engineering, University of Liverpool, Liverpool, L69 3GH, United Kingdom.
[4] Department of Materials Science and Engineering, The University of Tennessee, Knoxville, TN 37996, USA.

Oxides with generic stoichiometry M_7O_{12} occupy, in a generic phase diagram, an intermediate place between fluorite and bixbyite structure types. Their structure is derived from the ideal fluorite structure, and it is characterized by a more or less pronounced ordering of the O vacancies within the average fluorite sublattice. We believe that ternary oxides with this kind of formula provide interesting degrees of flexibility for understanding the structural characteristic of these structures in the context of fission product stabilization in nuclear fuels and in the field of actinide waste forms as well. We would like to discuss the structural characteristics of the chemical bonds in ternary systems consisting of trivalent and hexavalent cations. Eventually, in compounds with generic formula $Y_6B^{+6}O_{12}$, the B cation can be either a transition metal (W, Mo) or hexavalent uranium. We believe that studying the polyhedron of the sevenfold coordinated Y ion is particularly interesting to understand the flexibility of the chemical bonds: it is often described in the literature as a mono-capped trigonal prism, with bond lengths exhibiting an extremely large dispersion, ranging for instance from 2.19 to 2.70 Å in Y_6WO_{12}. We would discuss the implications of this large dispersion of distances on the chemical bond characteristics, compare DFT models with established experimental knowledge on pristine and irradiated specimens.

Introduction

Mixed oxides belonging to the RE_2O_3-BO_2 systems (RE is a are earth element and B is a tetravalent metal element) have been extensively explored because they display a variety of interesting effects, ranging from order-disorder phase transitions [1-4], to geometrically frustrated magnetism [5], and ionic conductivity [6]. They are encountered in a variety of technological applications, which include solid state electrolytes for fuel cells, thermal barrier coatings, neutron absorbing materials [7] and nuclear waste storage matrices [8-9]. The phase diagrams of these pseudo-binary systems often present a variety of phases related to the fluorite ideal arrangement, but with different structures [10-18] depending on the partial or complete ordering of O vacancies and the metal ions in their respective sublattices.

At the extremes of the pseudo-binary diagram, the simple oxides crystallize in the fluorite (BO_2) and the bixbyite structures (RE_2O_3). The fluorite phase is stoichiometric and displays a perfect face centered cubic arrangement of the atoms. The bixbyite phase comes with three flavors (A, B, and C) that have different symmetries: they roughly maintain the metal arrangement of the fluorite structure while the O vacancies order leads to the formation of a different polyhedral connectivity and two environments for the cations. Moving away from the bixbyite towards the middle of the phase diagram, weberite, pyrochlore, and O-rich bixbyite phases can be observed for the 1:1 ratio of the aliovalent cations. Often, the occurrence of a particular structure depends on the synthesis method, and not exclusively on the amounts of the specific initial oxides RE_2O_3 and BO_2. In several cases, kinetic factors as the annealing dwell and the quenching conditions can promote the formation of a specific phase.

Moving beyond the 1:1 ratio, closer to the fluorite phase, oxides with generic stoichiometry M_7O_{12} are often observed [19]. They possess a trigonal structure derived from the ideal fluorite structure, that displays a pronounced ordering of the O vacancies within the average fluorite sublattice. Depending on the respective charges of the two atoms, their generic formula can be $RE_4B^{+4}{}_3O_{12}$ or $RE_6B^{+6}O_{12}$. While both systems display highly ordered vacancies, the first system does not display significant cation ordering or site selectivity, while the second systems are perfectly ordered. The ordered compounds undergoing ion irradiation see their structure transforming from ordered rhombohedral to amorphous. In the ordered compounds (Y_6MoO_{12}, Y_6WO_{12}, …) a competitive oxygen deficient cubic fluorite phase can be observed at high temperature. This observation suggests the irradiation behavior (amorphization) is not following the path of the thermally driven polymorphism. The disordered compounds (as for instance $Sc_4Hf_3O_{12}$) do not become amorphous but they transform into an oxygen deficient long-range fluorite structure. Recently [14], we discovered the local structure rearranges according to an O excess bixbyite structure, suggesting a not random configuration of the O vacancies. In both systems, the change of crystal symmetry between the ordered rhombohedral and the irradiated phase is expected to involve a drastic change of the connectivity and coordination of the atom polyhedra, involving a possible semi-reconstructive character. It is therefore interesting to analyse the strength and the characteristics of the chemical bonds occurring in these polyhedra.
We believe that ternary oxides with this generic formula $(RE_{1-x}B_x)_7O_{12}$ can display an excellent structural flexibility to incorporate fission products and minor actinides, and eventually be interesting for the design of advanced nuclear fuels. This paper addresses the specificity of the chemical bonds of a particular subset of fully ordered compounds of chemical composition $Y_6B^{+6}O_{12}$ that can explain the reasons of the chemical and structural flexibility of these ordered and disorder members.

Materials and Methods

To examine the characteristics of the chemical bonds in a quantitative way, atoms-in-molecule (AIM) Bader's analysis method was used to model the electron density. The AIM-Bader analyses using AIM-UC software [20] provided estimates for the Bader charges of the individual atoms, as well as the locations of the bond critical points (BCPs) between bonding atoms, the charge densities at these BCPs, and the local curvature of the charge density. The analysis for each compound was performed according to the procedures described in [21]. DFT calculations were performed to obtain the electron charge densities for three compounds of interest in this paper: Y_6MoO_{12}, Y_6WO_{12}, and Y_6UO_{12}. For these calculations, we used the generalized gradient approximation Perdew-Burke-Ernzerhof (PBE) [22] exchange-correlation functional. The yttrium 4s4p5s4d, molybdenum 4p5s4d, tungsten 5p6s5d, uranium 6s6p5f6d7s, and oxygen 2s2p electrons were treated as valence electrons. The electron-ion interaction was described by the projector augmented wave method, and the plane-wave basis energy cutoff was set to 520 eV. The Vienna ab initio package VASP [23,24] was employed to perform the GGA calculations. GGA+U functionals within the simplified rotationally invariant approach introduced by Dudarev [25] were required to take into account the strongly correlated nature of the f states of uranium. An effective Hubbard parameter equal to 4eV was employed. A uniform 4x4x4 k-point mesh for the Brillouin zone sampling of the primitive trigonal rhombohedral cell was adopted based on the Monkhorst-Pack scheme. That choice was found to be sufficient to achieve well converged energies. Electronic self-consistency was considered achieved when the total energy change between electronic steps was less than ≤ 10μeV. The lattice metric was relaxed for all crystal symmetries and the internal structural parameters were relaxed until all Hellmann-Feynman forces on each ion were ≤ 3 meV/Å. Real space sampling of the charge density was performed on a regular 635x635x635 grid.

Results

Figure 1 reports the relaxed structural parameters of Y_6WO_{12} in the trigonal rhombohedral primitive lattice. A schematic representation of the structure is provided in the same figure, showing the particular connectivity of the 7-fold coordinated Y atoms.

Site	*x/a*	*y/b*	*z/c*	*Mult.*
Y	0.6843	0.3895	0.8563	6
B	0	0	0	1
O1	0.4313	0.1770	0.5917	6
O2	0.9225	0.7049	0.0341	6

R-3 space group.

a: ~ 6.475 Å, α: ~ 98.64°

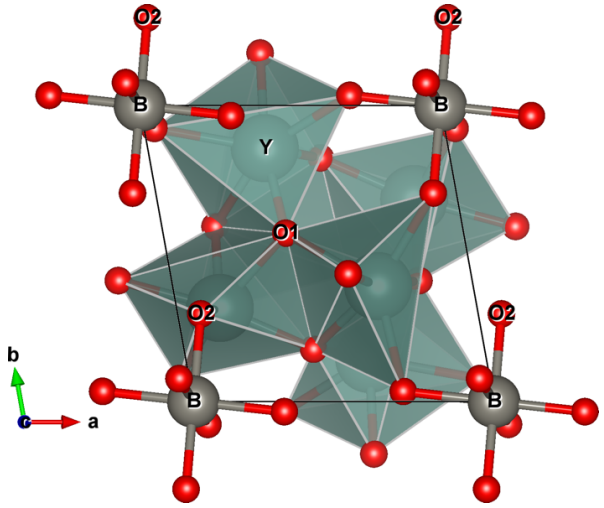

Fig. 1 Left panel: Atomic position of the fully relaxed structure of Y_6WO_{12} obtained by DFT calculation (B=W). Right panel: representation of the primitive rhombohedral trigonal structure.

The different characteristic of the charge density distribution for the two polyhedral can be displayed drawing same value isosurfaces of the charge density. The amount of charge density along the bonds of the BO_6 octahedron (for the three compounds) is much larger than the one observed in the YO_7 polyhedron (Fig.2).

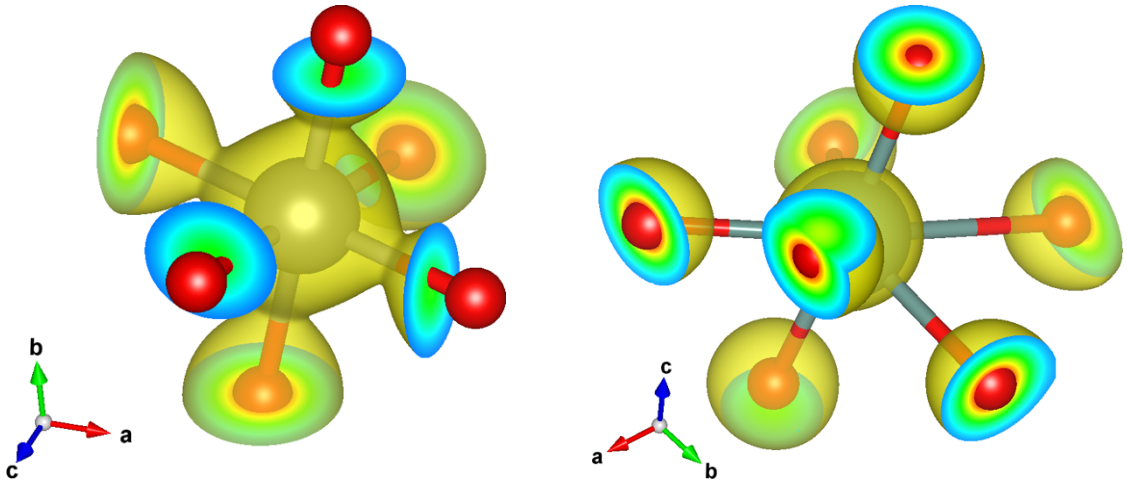

BO_6 (Mo, W, U) YO_7

Fig. 2 Contour maps showing the charge density distributions for the two polyhedra in the ordered δ-phase structures of Y_6MoO_{12}, Y_6WO_{12}, and Y_6UO_{12}.

The results of the Bader analysis of the charge density are reported in Table 1. The 6 identical bonds of the MO_6 octahedra are the shortest and the strongest in the three compounds. The 7 bonds of the yttrium environment are arranged according to their decreasing bond length and increasing strength. The 6 shorter bonds are medium to strong, but the extreme weakness of the longest bond is remarkable. This confers a quite interesting picture of a YO_7 polyhedron where one of the bonds with the atoms O atoms can be easily modified. This bond is increasingly weaker going from the Mo to the W, and finally to the U compound. The experimental Y-O distances in these three compounds display an excellent agreement with our DFT results. The Y-O bond lengths range from 2.19(1) to 2.70(1) Å for Y_6WO_{12} [26]. In Y_6UO_{12}, Y-O bond lengths range from 2.17(4) to 2.78(3) Å [27]. The delta phase polymorph of Y_6MoO_{12} [28] only occurs above 1670K, therefore a direct comparison with the experimental bond lengths of this phase is not straightforward because of the significant thermal expansion, but the compound retains the same structural features of the prototype Y_6WO_{12} compound.

Y_6MoO_{12}	**bcp density**	**curvature**	**laplacian**	**dist**
Mo-O1 x6	0.9718	0.2475	11.1031	1.950
Y-O1	0.1526	0.1655	2.0966	2.723
Y-O1	0.3028	0.2032	3.7058	2.481
Y-O1	0.3184	0.2068	3.9526	2.412
Y-O2	0.4057	0.2112	4.9286	2.337
Y-O2	0.4241	0.2136	5.2572	2.317
Y-O2	0.4701	0.2106	5.9289	2.256
Y-O2	0.5103	0.2104	6.7130	2.221
Y_6WO_{12}	**bcp density**	**curvature**	**laplacian**	**dist**
W-O1 x6	1.0041	0.2429	11.8996	1.957
Y-O1	0.1497	0.1645	2.0662	2.720
Y-O1	0.3012	0.2018	3.7216	2.460
Y-O1	0.3213	0.2088	3.9900	2.399
Y-O2	0.4069	0.2115	4.9402	2.323
Y-O2	0.4258	0.2131	5.2955	2.302
Y-O2	0.4698	0.2100	5.9504	2.249
Y-O2	0.5101	0.2085	6.7419	2.212
Y_6UO_{12}	**bcp density**	**curvature**	**laplacian**	**dist**
U-O1	0.9518	0.2730	7.9108	2.0956
Y-O1	0.1297	0.1584	1.7949	2.7831
Y-O1	0.3260	0.2084	4.0722	2.3744
Y-O1	0.3311	0.2041	4.1229	2.3735
Y-O2	0.3925	0.2162	4.5689	2.3122
Y-O2	0.4260	0.2115	5.2641	2.2752
Y-O2	0.4262	0.2078	5.3661	2.2712
Y-O2	0.4753	0.2087	6.0540	2.224

Table 1. Bader analysis of the charge density at the bond critical points for the three compounds.

The charge density of the seven Y-O bonds in the three compounds behaves according to a same master exponential curve (fig. 3), providing a direct correlation between bond strength (charge at the bcp) and bond length for this polyhedron. The analysis of the curvature (and the Laplacian) of the charge density along the bond direction confirms this conclusion.

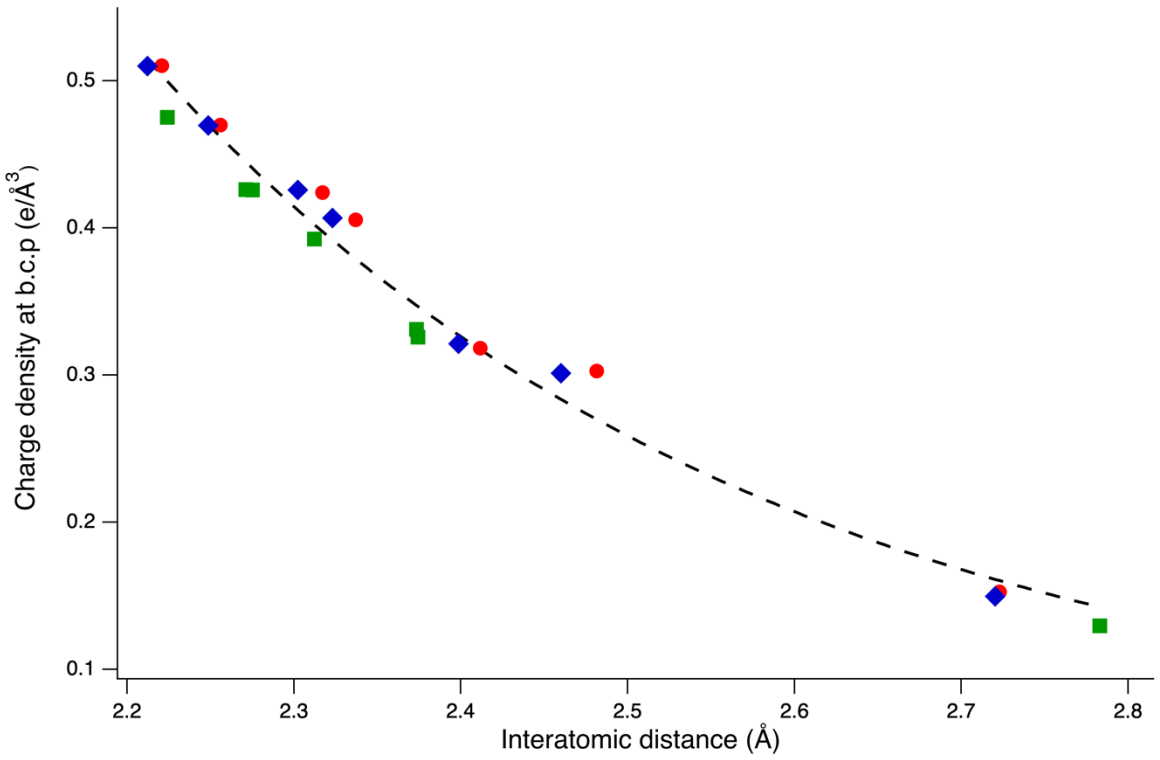

Fig. 3 Green squares represent the charge at the bcp of a given bond formed by Y atoms and oxygen in Y_6UO_{12}. Red dots are for Y_6MoO_{12}. Blue diamonds for Y_6WO_{12}. The dotted line is the simple exponential fit of the three sets of data.

Discussion

Bader analysis of the charge density of three ordered δ-phases allows to single out the particular weakness of one of the bonds formed by Y and O. This weak bond systematically concerns one of the O atoms that is also simultaneously bonded to the hexavalent metal. The effect is stronger (i.e. the bond is the weakest) in the uranium compound. We believe that the polymorphism observed at high temperature can be related of a polyhedron reshaping that is favored by this anisotropic characteristic of the bonds. This polyhedron reshaping is related to the modification of the ordered distribution of O vacancies on the anionic sub-network. Indeed, the perfect oxygen/vacancies ordering characteristic of the delta phase no longer occurs when the delta-phase structure is perturbed. This effect seems also likely to be transferable to the problem of the changes observed under irradiation in $Sc_4Hf_3O_{12}$ [14], where a large bond spread exists in the pristine samples and a drastic change of these bond lengths is observed after irradiation leading to a O vacancy arrangement similar to the one observed in bixbyite compounds. In the Y_6MoO_{12} compound, a competition between bixbyite and delta phase structures as a function of T, aliovalent doping, and sintering conditions is also observed [29], leading to a similar modification of the O vacancy distributions, involving the modification of the longer Y-O bond of the YO_7 polyhedron. This weakness of the sevenfold coordinated polyhedra can be an interesting parameter for designing materials that must withstand intense irradiation, where the flexible environment can reconstruct, can help healing the radiation damage, and thus increase the radiation tolerance of these system.

The authors declare no competing interests. The datasets generated during and analysed during the current study are available from the corresponding author on reasonable request.

References

1. D. J. M. Bevan, L L. Martin and R. L. Martin. The role of the coordination defect (CD) in the structures of anion-deficient, fluorite-related compounds. Acta Cryst. B69 (2013) 17-29.
2. E. Andrievskaya, Phase equilibria in the refractory oxide systems of zirconia, hafnia and yttria with rare-earth oxides, J. Eur. Ceram. Soc. 28 (2008) 2363-2388.
3. E. Isupova, V. Glushkova, E. Keler, A study of the Gd_2O_3-HfO_2 system in the composition range enriched with hafnia, Izv. Akad. Nauk. SSSR, Neorg. Mater. 4 (1968) 1732-1737.
4. M. Subramanian, G. Aravamudan, G. Subba Rao, Oxide pyrochlores : a review, Prog. Solid State Chem. 15 (1983) 55-143.
5. J. Gardner, M. Gingras, J. Greedan, Magnetic pyrochlore oxides, Rev. Mod. Phys. 82 (2010) 53.
6. H. Yamamura, H. Nishino, K. Kakinuma, K. Nomura, Electrical conductivity anomaly around fluorite-pyrochlore phase boundary, Solid State Ionics 158 (2003) 359-365.
7. V. Risovany, A. Zakharov, E. Muraleva, V. Kosenkov, R. Latypov, Dysprosium hafnate as absorbing material for control rods, J. Nucl. Mater 335 (2006) 163-170.
8. R. Ewing, W. Weber, J. Lian, Nuclear waste disposal e pyrochlore (A2B2O7): nuclear waste form for the immobilization of plutonium and "minor" actinides, J. Appl. Phys. 95 (2004), 5949-5071.
9. K. Sickafus, R. Grimes, J. Valdez, A. Cleave, M. Tang, M. Ishimaru, S. Corish, C. Stanek, B. Uberuaga, Radiation-induced amorphization resistance and radiation tolerance in structurally related oxides, Nat. Mater 6 (2007) 217.
10. J. Shamblin, M. Feygenson, J. Neuefeind, C. Tracy, F. Zhang, S. Finkeldei, D. Bosbach, H. Zhou, R. Ewing, M. Lang, Probing disorder in isometric pyrochlore and related complex oxides, Nat. Mater. 15 (2016) 507-511.
11. E. O'Quinn, K. Sickafus, R. C. Ewing, G. Baldinozzi, J. Neuefeind, M. Tucker, A. Fuentes, D. Drey, M. Lang. Predicting short-range order and correlated phenomena in disordered crystalline materials. Sci Adv. 6 (2020) eabc2758
12. P. Blanchard, R. Clements, B. Kennedy, C. Ling, E. Reynolds, M. Avdeev, A. Stampfl, Z. Zhang, L.-Y. Jang, Does local disorder occur in the pyrochlore zirconates? Inorg. Chem. 51 (2012) 13237-13244.
13. L. Cai, J.C. Nino, Complex ceramic structures. I. Weberites. Acta Cryst. B65 (2009). 269-290.
14. M. K. Patel, K. E. Sickafus, G. Baldinozzi, Divergent short- and long-range behavior in ion-irradiated δ−$Sc_4Hf_3O_{12}$. Phys. Rev. Materials 4 (2020) 093605. DOI: 10.1103/PhysRevMaterials.4.093605
15. DL Drey, EC O'Quinn, T Subramani, K Lilova, G Baldinozzi, IM Gussev, A. F. Fuentes, J. C. Neuefeind, M. Everett, D. Sprouster, A. Navrotsky, R. C. Ewing, M. Lang. Disorder in $Ho_2Ti_{2-x}Zr_xO_7$: pyrochlore to defect fluorite solid solution series. RSC Advances 10 (2020), 34632-34650
16. P. Blanchard, S. Liu, B. Kennedy, C. Ling, M. Avdeev, J. Aitken, B. Cowie, A. Tadich, Investigating the local structure of lanthanoid hafnates $Ln_2Hf_2O_7$ via diffraction and spectroscopy, J. Phys. Chem. C 117 (2013) 2266-2273.
17. M.K.Patel, G. Baldinozzi, J.A. Aguiar, J.A. Valdez, S. C. Vogel, K. E. Sickafus. Structural analysis of $Gd_2Ce_2O_7$. MRS Online Proceedings Library 1743 (2015) 7-13. DOI: 10.1557/opl.2015.142
18. C. Stanek, C. Jiang, B. Uberuaga, K. Sickafus, A. Cleave, R. Grimes, Predicted structure and stability of $A_4B_3O_{12}$ δ-phase compositions, Phys. Rev. B 80 (2009), 174101.
19. D. J. M. Bevan, J. Mohyla, K. S. Wallwork, H. J. Rossell, E Schweda. Structural Principles for Anion-Deficient, Fluorite-Related Superstructures in the Zirconia-Scandia System. Zeitschrift für anorganische und allgemeine Chemie 628 (2002) 1180-1186.
20. D. Vega, and D. Almeida. AIM-UC: an application for QTAIM analysis. Journal of Computational Methods in Sciences and Engineering 14 (2014) 131-136. DOI: 10.3233/JCM-140491

21. L. Casillas-Trujillo, G. Baldinozzi, M Patel, H. Xu, K. Sickafus. Comparison of bonding and charge density in δ−UO_3 , γ−UO_3, and La_6UO_{12}. Phys. Rev. Materials 1 (2017), 65404. DOI: 10.1103/PhysRevMaterials.1.065404
22. J. P. Perdew, J. Chevary, S. Vosko, K. A. Jackson, M. R. Pederson, D. Singh, and C. Fiolhais, Atoms, molecules, solids, and surfaces: Applications of the generalized gradient approximation for exchange and correlation, Phys. Rev. B 48 (1993), 4978.
23. G. Kresse and J. Furthmüller, Efficiency of ab-initio total energy calculations for metals and semiconductors using a plane-wave basis set, Comput. Mat. Sci. 6 (1996) 15.
24. G. Kresse and J. Hafner, Ab initio molecular dynamics for liquid metals, Phys. Rev. B 47 (1993) 558.
25. S. L. Dudarev, G. A. Botton, S. Y. Savrasov, C. J. Humphreys, and A. P. Sutton. Electron-energy-loss spectra and the structural stability of nickel oxide: An LSDA+U study. Phys. Rev. B 57 (1998) 1505.
26. N. Diot, P. Bénard-Rocherullé, and R. Marchand. X-ray powder diffraction data and Rietveld refinement for Ln_6WO_{12} (Ln=Y, Ho). Powder Diffraction, 15 (2000) 220-226
27. S. F. Bartram. Crystal Structure of the Rhombohedral MO_3:$3R_2O_3$ Compounds (M = U, W, or Mo) and Their Relation to Ordered R7O12 Phases. Inorganic Chemistry, 5 (1966) 749-754.
28. D. Schildhammer, G. Fuhrmann, L. L. Petschnig, G. Partl, T. Götsch, S. Penner, Andreas Schaur, A. Saxer, H. Schottenberger, and H. Huppertz, Cubic Bixbyite-Structured Phases of Yb_6MoO_{12} and Y_6MoO_{12} Prepared by the Solution Combustion Method at Low Temperatures. European Journal of Inorganic Chemistry, 15 (2017) 2265-2269.
29. P. Sobota, M. Guzika, V. Garnier, G. Fantozzi, M. Sobota, E. Tomaszewicz, Y. Guyot, and G. Boulon. Fabrication of Y_6MoO_{12} molybdate ceramics: from synthesis of cubic nano- powder to sintering. Ceramics International 46 (2020) 4619-4633.